An Automated Radiometer Traversing System for Use in a Model Urban Canyon

J. A. VOOGT AND D. G. STEYN

Atmospheric Science Program, Department of Geography, The University of British Columbia, Vancouver, B.C., Canada

(Manuscript received 27 July 1990, in final form 8 December 1990)

ABSTRACT

The design of an automated radiometer traversing system used to measure nocturnal longwave surface radiative budgets in a model urban canyon is described. The system allows two net radiometers to be traversed around the perimeter of a canyon cross section in order to resolve the spatial distribution of net radiation without necessitating extensive arrays of instruments. The system has been used to study the temporal and spatial variations of radiation and near surface air temperature within a model urban canyon and to validate a numerical canyon radiation model. Considerations affecting the placement of the sensors with respect to the canyon surfaces are detailed. The traversing speed is determined using an analysis of sensor response to anticipated spatial changes in radiation across canyon surfaces. Test results confirm the design parameters.

1. Introduction

Field observation programs designed to study the microscale meteorology of urban canyons are faced with the difficulty of selecting an appropriate, representative location at which observations may be made, and are often limited by numerous logistical constraints. Substantial spatial variations in meteorological variables often occur within urban canyons, necessitating extensive arrays of instrumentation (e.g., Nunez and Oke 1977; Nakamura and Oke 1988). One alternative that has been used to overcome some of the real-world restrictions inherent in the study of urban canopy-layer climate is the use of scale models. Oke (1981) and Johnson and Watson (1987) have used scale models to study the influence of canyon geometry upon surface radiative cooling, and Aida (1982) examined the albedo of canyon systems. The instrumentation used in those studies was very simple, in part owing to the much reduced scale of the models, and consisted of single (Oke 1981) or multiple (Johnson and Watson 1987) thermocouples and one upright and one inverted pyranometer (Aida 1982). The measurements obtained were thus an integrated value over the entire model surface and do not address the subcanyon-scale variability within individual canyons. The use of a larger scale model in which more extensive within-canyon instrumentation could be employed would allow the microscale variation of climate elements within canyons to be studied.

Recently, such a model has been constructed (Voogt 1989). It incorporates an automated canyon traversing system (CTS), an apparatus used to traverse radiometers around a model urban canyon cross section in order to obtain spatially resolved radiation measurements on each of the canyon facets (walls, floor, and top). The use of the CTS allows the spatial and temporal variations of the nocturnal longwave radiation balance to be resolved in a reduced-scale canyon without the need for multiple instruments that are prohibitive in cost and the space they would occupy in the scale model. It also eliminates the need to match instruments. The model canyon and CTS have been used to perform a validation test of the Arnfield (1976, 1982) numerical urban-canyon radiation model (Voogt 1989; Voogt and Oke 1990) for nocturnal longwave fluxes and to investigate the spatial and temporal variations of the nocturnal cooling of canyon surfaces (Voogt 1989). Further development of the CTS to carry a variety of sensors for investigating other processes of interest in the urban canopy layer is possible.

This paper describes the design of the automated traversing system and the scale canyon in which it was used. Test results from the CTS are presented.

2. A simple model urban canyon

a. Description

The model canyon was constructed outdoors and comprised two identical walls approximately 10 m long with a maximum height of 1 m oriented north–south on an existing base of poured concrete. Each wall was constructed using a stack of between three and five overlapping layers of 200 × 200 × 400 mm^3 two-cell, hollow concrete blocks, capped by a single layer of 200

Corresponding author address: Mr. James A. Voogt, Atmospheric Science Programme, Depts. of Geography and Oceanography, University of British Columbia, 218-1984 West Mall, Vancouver, British Columbia, CANADA V6T 1Z2.

$\times 200 \times 50$ mm^3 solid concrete slabs, depending upon the desired height to width ratio (H/W). Standard overlapping brick construction was used to build the walls. That a wall length of 10 m was an adequate representation of an "infinitely long" wall is justified in Fig. 1. The maximum canyon width that could be used with the CTS was 1.9 m; the minimum width was approximately 0.5 m. Canyon H/W was varied in all but one case (0.41) by varying the width rather than the height. This method was adopted because the CTS allowed more variability in the length of the traverse than in the height.

A supporting framework was not used in the canyon construction and the blocks were not joined by any bonding material. No adhesives were used because tear down and rebuilding of the wall was necessary to generate new values of H/W. A 25-mm layer of extruded polystyrene insulation was taped to the exterior of the walls to aid in isolating the inner, active canyon surfaces by reducing heat loss through the backs of the canyon walls and by reflecting incident shortwave radiation on the outside of the walls.

b. *Similarity*

Similarity with real-world canyons is limited to the geometric similarity obtained through the use of H/W. Canyon materials and construction techniques have not been explicitly scaled, although they bear some resemblance to those found in real deep urban canyons where the surrounding buildings are largely made up of concrete or other materials with high thermal admittance. Processes governing radiative transfer have not been scaled in any way. As in Oke (1981), the characteristic length scale of radiative transmission may be considered to be negligible compared to the length scales of the model. The path length available for gaseous absorption and reemission of radiation within the canyon is less than that available in the real world and is not scaled. The time available for canyon heating and cooling is governed by natural factors.

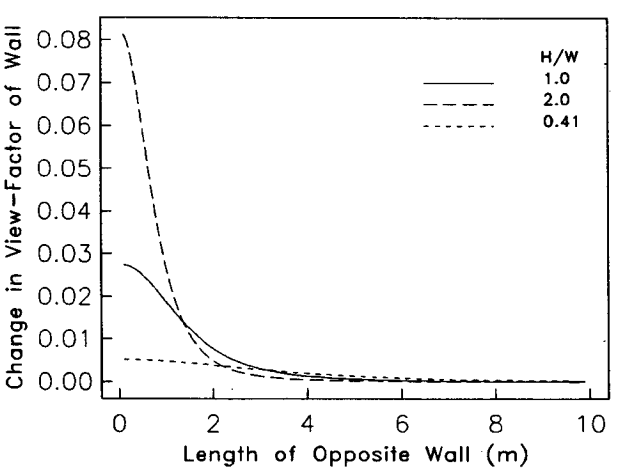

FIG. 1. The increase in wall view factor calculated for a point located midway up the opposite canyon wall at midcanyon for increasing lengths of wall.

c. *Restriction of results*

In addition to the scaling limitations discussed previously, there are other restrictions inherent in the use of the selected methodology, which may limit the extension of the scale model canyon results to full-size urban canyons. The scale model canyon does not include any interior heat source, so that results are limited to periods when canyon surface temperatures are not greatly affected by internal heat sources such as space heating. The current use of net radiometers with the CTS has been limited to nocturnal periods in which shading of directly irradiated surfaces by the sensors is not a problem. It is not expected that turbulent fluxes from this canyon would be comparable to those in the real world due to the dependence of the laminar boundary layer thickness upon the distance from the leading edge. The determination of CTS operating parameters was based on modeled longwave distributions characteristic of stable, clear, and light wind conditions in a symmetric canyon with $H/W = 1.0$. Those conditions were shown to generate large spatial differences of longwave radiation in the $H/W = 1.0$ canyon.

3. The canyon traversing system

a. *Description*

Figure 2 shows a generalized side view of the CTS as mounted in the model canyon and an end view of the vertical traversing assembly. The numbered labels correspond to those used in the following description.

The CTS uses two electric motors 1) and 2) to provide power for horizontal 3) and vertical 4) precision ball screws that drive an instrument carriage 5) around the canyon cross section. The length of the horizontal ball screw 3), limits the maximum canyon width, which may be used with the CTS. A third motor 6), mounted on the carriage, is used to rotate the two miniature radiometers 7). The arc of rotation required by the traversing instruments limits the minimum useful canyon width to approximately 0.5 m. Control and power are provided via a panel mounted behind the east wall of the canyon. The ball screws are mounted in a framework 8) bolted to the ground outside the canyon and stiffened by a guide wire 9) running through the walls across the bottom of the canyon. Electromechanical limit switches 10) govern the length of travel of the instrument carriage and are used to trip the rotation and delay sequence of the instruments. The traverse path for the instruments was: up the east wall; across the canyon top from east to west; down the west canyon wall; and across the canyon floor to the east wall. Upon reaching the end of each facet traverse, the instrument carriage trips a limit switch that

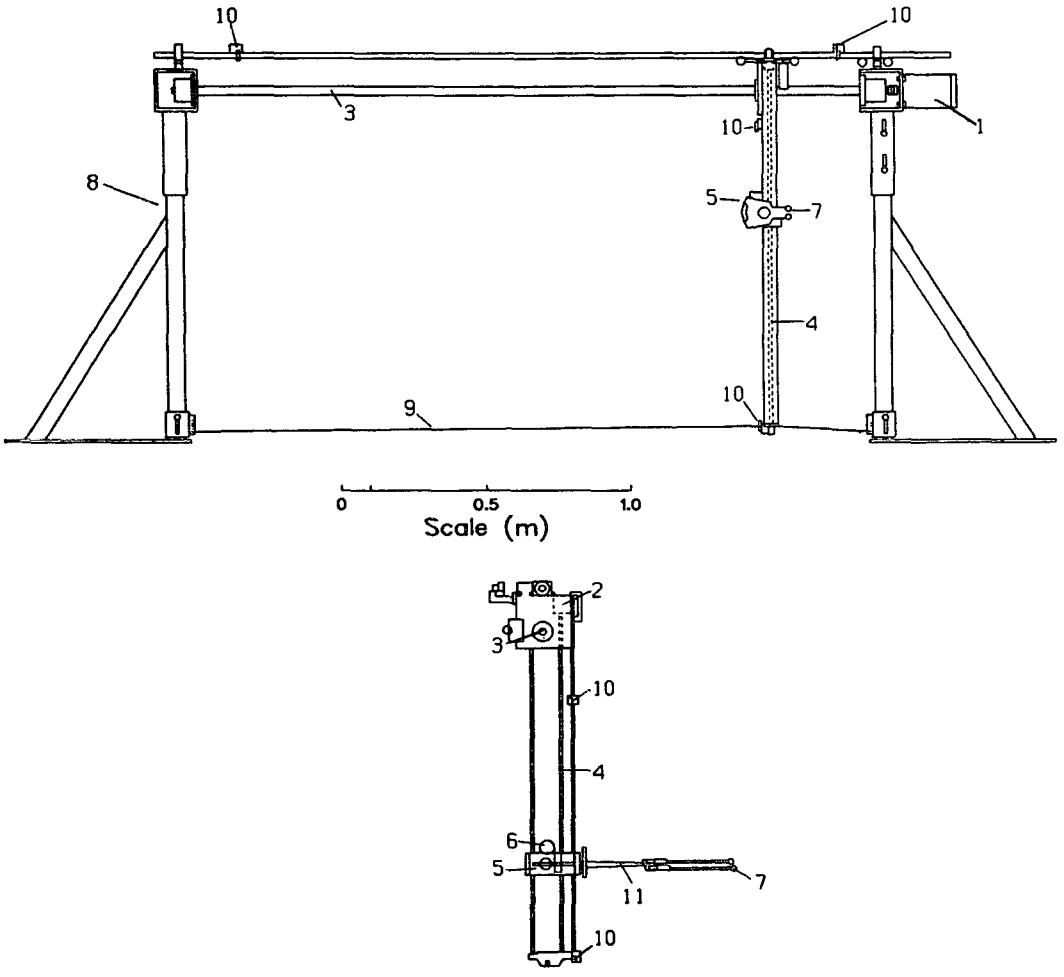

FIG. 2. Generalized drawing of the CTS. Top: side view; bottom: end view of the vertical traversing assembly. The numbered labels correspond to those used in the text description: 1) horizontal drive motor, 2) vertical drive motor, 3) horizontal drive screw, 4) vertical drive screw, 5) instrument carriage, 6) instrument rotation motor, 7) miniature radiometers, 8) support frame, 9) guidewire, 10) limit switches, 11) instrument carriage arm.

rotates the radiometers to face the new facet. The instrument carriage then remains stationary for a set period (the delay) prior to the commencement of traversing in order to allow the instruments to equilibrate to the new radiation balance. The radiometers are mounted on an arm 11) extending outward from the traversing carriage to reduce obstruction of the instrument's view factor by the CTS. Figure 3 shows the CTS mounted in the model canyon at the field site.

Manual and automatic modes of operation are available. Manual operation provides individual control over each motor so that the instrument carriage may be placed anywhere within the canyon cross-section boundaries defined by the limit switches. During automatic operation, the instruments traverse around the canyon cross section, while automatic instrument rotation and delays are engaged via the limit switches. This was the primary mode used for data collection.

The sensor position may be determined at any point through knowledge of three parameters: traverse speed, state of the traverse (delay or traversing), and start location. The state of the traverse is indicated by a voltage at the control panel (high when the traversing system is in a delay and low otherwise), which is recorded to indicate the state of the traverse.

The distance between the radiometer sensing surface and the canyon facet being traversed averages 30–40 mm for the walls and 20 mm for the canyon floor. The instruments are set coincident with the plane across the canyon top.

b. Traversed instruments

In the configuration employed, the traversed sensors include two miniature net radiometers (Swissteco Model S1 Minor Mk 2) and a 30 awg type-T unshielded thermocouple for monitoring air temperature.

One of the radiometers was equipped with a black-

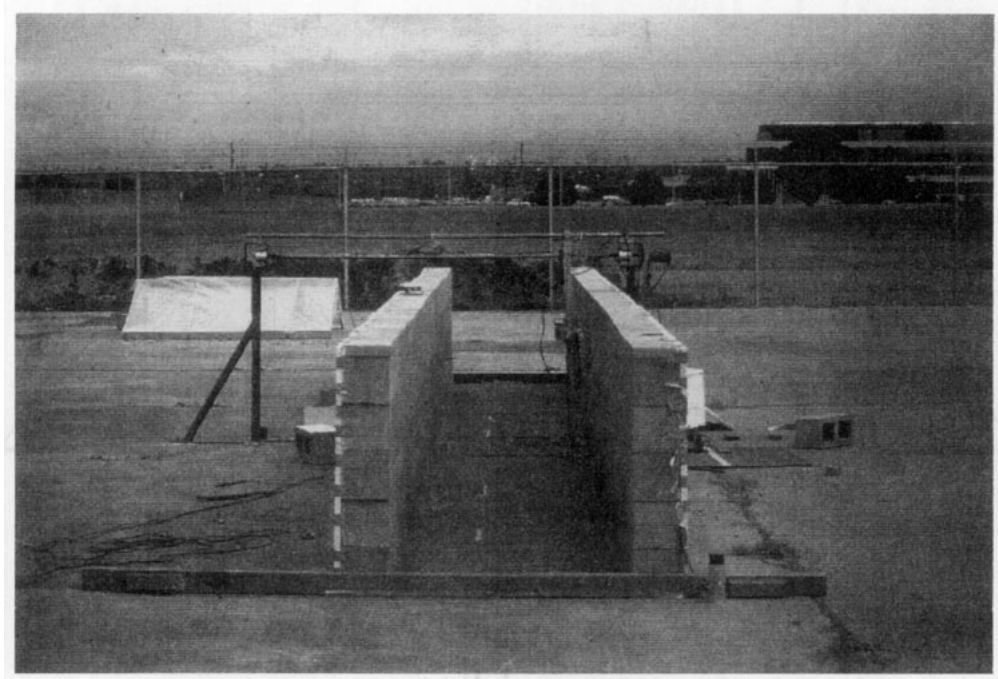

FIG. 3. The CTS as mounted in the model canyon.

body cavity in order to measure the outgoing longwave radiation (L_o) from the canyon walls and floor. The second was operated in a net radiation configuration to measure L^*. The outgoing longwave radiation L_o was measured in preference to the incoming longwave flux (L_i) because the height of the instrument dome is less than that of the blackbody cavity and therefore allows the instrument to be located closer to the canyon surface.

Table 1 compares the instrument specifications of the more commonly used full-size Swissteco S1 net radiometers with those of the miniature version. Advantages of using the miniature radiometers include: reduced power and strength requirements for the CTS, a reduction in the canyon volume taken by instrumentation and therefore a reduction in the view factor of the instrumentation, and the ability to locate the radiometers much closer to the surface due to the smaller domes used on the instruments. As the radiometers are positioned closer to the surface of measurement, errors due to emission by the intervening air layer are reduced (Idso and Cooley 1971). In the nocturnal urban-canyon environment, this is of importance in the early evening when surface temperatures can be significantly different from air temperatures.

TABLE 1. Miniature and full-size net radiometer specifications. Source: Miniature (W. Beerli, personal communication), full-size (Monteith 1972).

Parameter	Miniature S1 minor Mk 2	Full size S1
Diameter of sensing surface	16 mm	50 mm
Instrument diameter	22 mm	95 mm
Height of dome above sensing surface	10 mm	30 mm
Sensitivity (typical)	0.006 mV W^{-1} m^2	0.04 mV W^{-1} m^2
Accuracy of calibration	±2.5%	±2.5%
Response time	98% in 22 s	98% in 25 s

c. *Specification of the traverse separation distance*

The design of the traverse separation distance (distance separating the sensor from the surface to be measured) is based upon view factor considerations and the height of the canyon wall. The radius of the area seen by a radiometer at a separation distance necessary to achieve a given view factor is shown graphically in Fig. 4. It emphasizes that as the instrument separation distance above the surface decreases, a smaller area provides a given view factor. This is an important consideration when using the CTS for numerical model validation because models such as Arnfield (1982) predict the flux density for a specific point on the surface, while a radiometer measures the average flux density for the area viewed.

The view factor of the surface becomes critical near the ends of the facets, particularly the tops of the canyon walls. With increasing separation distances in these regions, an increasing proportion of the instrument's view factor will be occupied by a facet other than that being

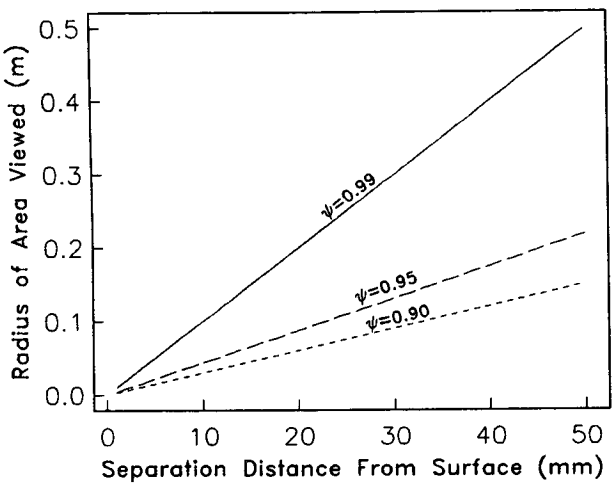

FIG. 4. Radius of the area seen by a radiometer necessary to achieve a given view factor for different separation distances from the surface.

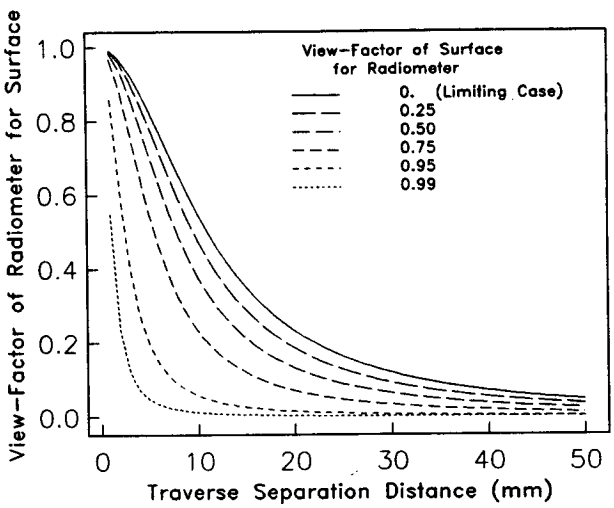

FIG. 6. Obstruction of the radiation field by a miniature radiometer located above a canyon surface. View factors are calculated for a point directly beneath the radiometer (limiting case) and for the circular areas that make up the surface view factor of the instrument.

traversed, or, in the case of the tops of the walls, the night sky. Figure 5 illustrates this "end effect" as a traversing radiometer approaches the end of a 1.0-m canyon wall.

The lower limit of the traverse separation distance is determined by the roughness of the surface and the height to which the instrument domes project above the sensing surface. However, the placement of a radiometer close to the surface obscures a portion of the radiation field that would normally be viewed at that point (Fig. 6) and replaces the L_i from the sky, walls, and floor with L_i emitted from the radiometer. This will affect the radiative balance of the surface being measured if the temperature of the radiometer differs from that of the surroundings and will have a larger effect as the sensor is positioned closer to the surface; i.e., the view factor of the radiometer for the surface increases.

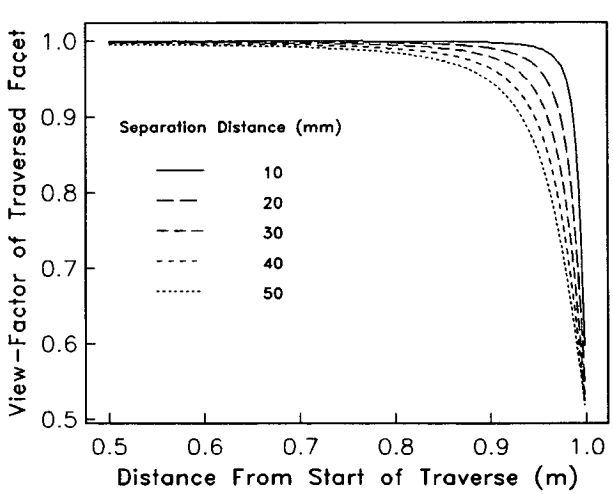

FIG. 5. The "end effect" for view factors of a traversed canyon facet as a traversed radiometer approaches the end of a facet. The effect is diminished at lower traverse separation distances.

In tests conducted by Idso and Cooley (1972), no gradients were found in the surface temperature beneath a full-size radiometer located 0.2 m above a grass surface. Similar tests were repeated in this study for miniature and full-size radiometers mounted 50 mm above an open asphalt surface for an extended period of time. No discernible surface temperature changes were detected using a narrow-view infrared radiation thermometer (Barnes Model PRT 4A). Within a canyon the effect is likely to be small because the sky view factor, ψ_s, for points is already very much reduced, and the differences in radiative temperature between the radiometer and canyon surfaces are small compared to differences between radiometer temperatures and the sky radiative temperature. Any change in surface temperature occurring in the small area with a high view factor for the radiometers, which might be sensed by a narrow field-of-view instrument such as the PRT 4A, will be less evident in the signal from the net radiometers because they have a full hemispheric field of view. The likelihood of such changes occurring when the instruments are traversed is small. Thus, the instruments were positioned as close as possible to the canyon facet surfaces being traversed.

d. Specification of the instrument traversing speed

The sensor traversing speed was determined from an analysis of sensor response to anticipated changes in the outgoing and net longwave flux densities across canyon facets. The approach is based upon the response of a temperature sensor (first-order responder) to changes in environmental temperature as described in

Fritschen and Gay (1979). The time constant τ of the miniature radiometers used is 5.62 s, (22 s for 98% response, Table 1) calculated from

$$[Q(t) - Q_f]/(Q_0 - Q_f) = a = e^{-t/\tau}, \quad (1)$$

where Q_0 is the initial radiation, $Q(t)$ is the radiation at the time elapsed t, Q_f is the radiation following the step change, τ is the time constant of the instrument, and a is defined as the adjustment remaining.

The method described by Fritschen and Gay (1979) assumes a stationary instrument responding to a temporal change in the environmental temperature. Here it is assumed that spatial changes in radiation occurring over the length of a traverse are much greater than temporal changes; i.e., the change in L_o or L^* across a canyon facet is much larger than any change induced by heating or cooling in the time it takes to traverse the facet. The response of the instrument is, therefore, a function of distance, but can be related to time by the traversing speed.

The equation governing sensor response is

$$dQ/dt = -(Q - Q_A)/\tau, \quad (2)$$

where dQ/dt is the change of measured radiation with time (here time is the time necessary to traverse a facet and represents spatial rather than temporal changes), and Q_A is the actual or true radiation. If changes in Q_A over the facets are known, the sensor response may be calculated for the traverses across the canyon facets.

To obtain a first-order estimate of Q_A and the spatial distribution of longwave radiation over the canyon facets, modeled distributions of L_o and L^* were generated using the Arnfield (1976; 1982) model and a set of canyon temperature data collected from a canyon with $H/W = 1.0$ (Fig. 7). These data represent clear, light wind conditions in which large spatial changes of radiation were observed. The modeled measurements were substantiated by spot measurements of L_o and L^* taken by a miniature radiometer. The net and outgoing radiation distribution on the walls for most times after sunset may be represented by a linear ramp change and that of the top and floor by a ramp or part of a periodic function.

With a linear ramp change of L_o or L^*, the change of the radiation sensed by the radiometer over time (i.e., distance/speed) may be written

$$dQ/dt = -(Q - Bt)/\tau, \quad (3)$$

where B is the rate of change of the true radiation Q_A with time. To obtain (3), it is assumed that $Q = Q_A = 0$ at $t = 0$, and further, $Q_A = Bt$. Following Fritschen and Gay (1979), the solution of (3) with $Q = Q_A$ at the start of the traverse is

$$Q = Bt - B\tau(1 - e^{-t/\tau}), \quad (4)$$

and since $Q_A = Bt$,

$$Q - Q_A = -B\tau(1 - e^{-t/\tau}). \quad (5)$$

When $t \gg \tau$ (i.e., the traversing time is much greater than the instrument time constant), the second term on the right-hand side of (5) is reduced to 1 and the equation becomes linear.

Given an estimate of the change of L_o or L^* over the wall (ΔQ_A) and the speed of traverse, the slope B may be calculated. Specifying the length of traverse and instrument time constant, various speeds or times of traverse may be tested for the difference between Q and Q_A. Two such tests are presented in Table 2 and cases from each test are illustrated in Fig. 8.

With greater ΔQ_A and with faster traversing times, Table 2 shows that the difference between the true and measured radiation grows. The two ΔQ_A tested are representative of the modeled spatial changes of L^* and L_o times, early and late in the evening in a model canyon with $H/W = 1.0$ under clear, light wind conditions. The traversing times tested were chosen somewhat arbitrarily but are constrained by a lower limit, governed by the maximum speed of the traversing unit and the increase in vibrations of the sensors that accompany higher traversing speeds, and an upper limit, restricted by the total amount of time needed to complete an entire traverse. To maintain the difference ($Q - Q_A$) below -1 W m^{-2} for a ΔQ_A of 30 W m^{-2}, a speed of less than 5.95×10^{-3} m s^{-1} is necessary over a wall with a height 1.005 m.

For a sinusoidal change, the governing equation (3), assuming $Q = Q_A = 0$ at $t = 0$ and $Q_A = Q_1 \sin\omega t$, may be rewritten as

$$dQ/dt = -(Q - Q_1 \sin\omega t)/\tau, \quad (6)$$

where $\omega = 2\pi/\text{period}$ represents the angular frequency of oscillation, and Q_1 is the amplitude of the oscillations. The solution of the first-order linear differential equation with the constant solved for $Q = Q_A = 0$ at $t = 0$ as before, yields

$$Q = Q_1\omega\tau a e^{-t/\tau} + Q_1 a \sin[(\omega t - L)], \quad (7)$$

where

$$a = [1 + (\omega\tau)^2]^{-1/2} \quad (8)$$

and

$$L = \arctan(\omega\tau). \quad (9)$$

When $t \gg \tau$, a represents the attenuation factor of the measured signal and L/ω represents the time lag of the measured signal behind that of the true signal. The attenuation, lag, and lag time calculated at several traversing speeds are presented for sinusoidal radiation data with an amplitude of 10 W m^{-2} in Table 3. This amplitude is large with respect to most observed changes across the top and floor. Figure 9 illustrates the lag and attenuation for three traversing speeds.

For traverse times of 180 s or greater (5.56×10^{-3} m s^{-1} over a 1.005-m facet), the amount of attenuation is negligible and the lag times are small. As traverse

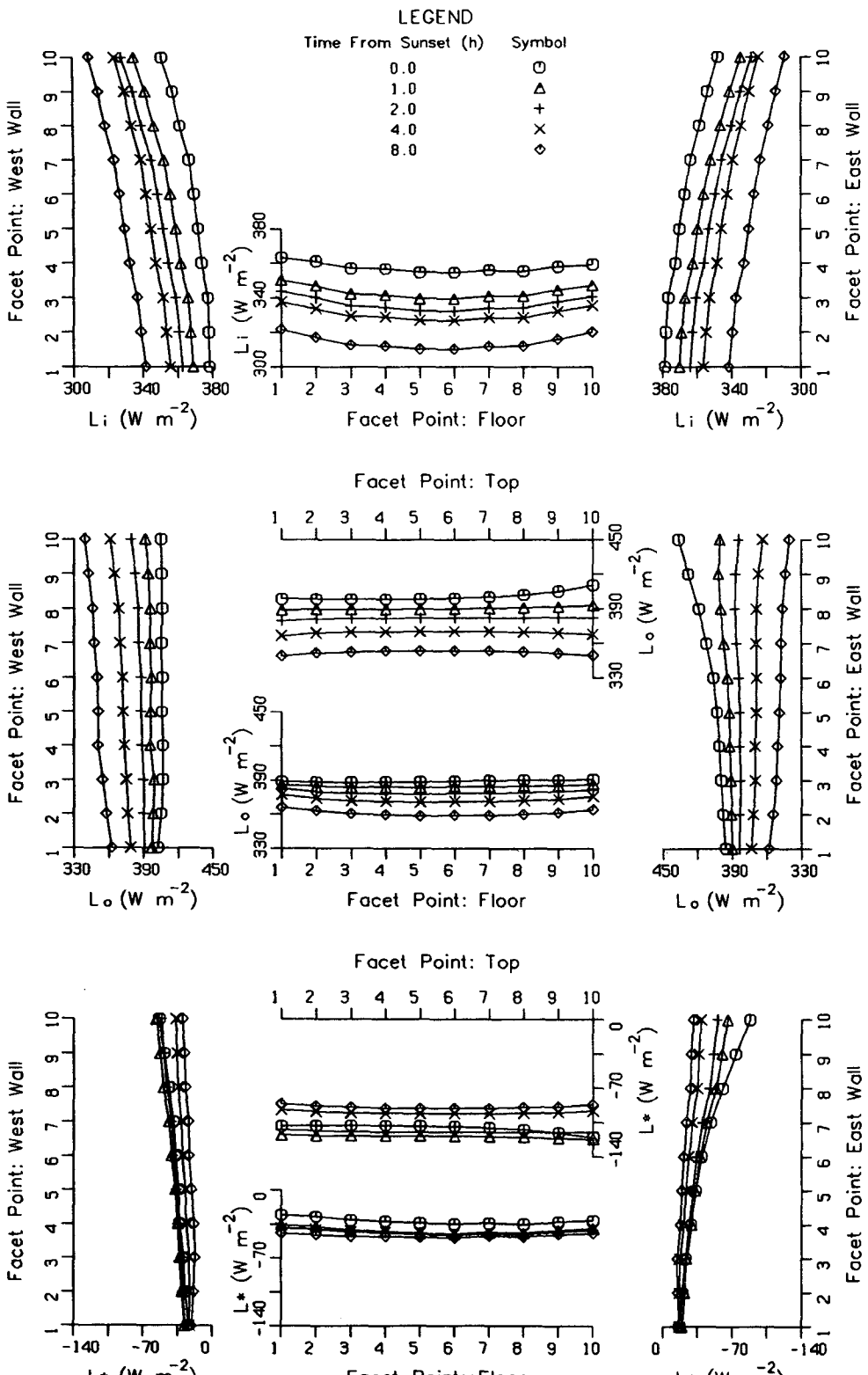

FIG. 7. Modeled distributions of L_i (top), L_o (middle), and L^* (bottom) over canyon facets for 10 October 1987 used for determining sensor traversing speed.

TABLE 2. True and measured radiation for a sensor traversed across a canyon wall. Change in flux density of radiation over a wall (ΔQ_A) is: (a) 15 W m^{-2}, (b) 30 W m^{-2}.

Traverse time (s)	Speed (m s^{-1}) $\times 10^{-2}$	Slope B (W m^{-2} s^{-1})	$\lvert Q - Q_A \rvert$ (W m^{-2})
(a)			
300	0.335	0.05	0.28
240	0.419	0.0625	0.35
180	0.558	0.0833	0.47
120	0.838	0.125	0.70
60	1.675	0.25	1.41
(b)			
300	0.335	0.10	0.56
240	0.419	0.125	0.70
180	0.558	0.167	0.94
120	0.838	0.25	1.41
60	1.675	0.50	2.81

times drop below 120 s (speeds less than 8.38×10^{-3} m s^{-1}), the attenuation becomes more pronounced and lag times decrease.

On the basis of the tests presented in Tables 2 and 3 and anticipated distributions of longwave radiation in canyons of differing H/W ratios, a constant traversing speed of 0.558×10^{-2} m s^{-1} over all facets was selected for operational use with the CTS. The CTS may also be configured so that vertical and horizontal traverses are conducted at different speeds, since separate drive motors are used but the speed remains constant over the traverse. It should be stressed that the analysis presented serves only as a guide to choosing an appropriate traversing speed and does not provide any form of correction factor. It is based on simple approximations to the actual radiation distributions that occur across canyon facets.

TABLE 3. Attenuation and lag time of canyon floor/top data for various traverse times. Amplitude of Q_A is 10 W m^{-2}.

Traverse time (s)	Period (s)	Attenuation factor	Lag	Lag time (s)
300	600	0.998	0.059	5.617
240	480	0.997	0.073	5.614
180	360	0.995	0.098	5.606
120	240	0.989	0.146	5.583
60	120	0.959	0.286	5.469

To test if the radiometers accurately measure the changing radiation while traversing at the selected speed, a single net radiometer was set in a fixed position over a canyon facet, and the measurements were compared to those of the traversed instruments as they passed the point. By necessity, the fixed radiometer was offset from the track of the traversed radiometers so that the areas viewed by the two instruments differed slightly. The comparison between the fixed and traverse estimates of L_o for the west wall (Fig. 10) indicate a slight overestimate by the traversing radiometer. The error bars on the traverse results are the standard deviations from the average value for all samples taken within the gridpoint boundaries of the point being tested. The error bars for the fixed radiometer data represent the standard deviation from the average value over the time taken for the traverse. The fixed radiometer output is a 1-min average, thus the standard deviations are generally small.

Figure 10 illustrates the results from two tests. In the first, the fixed radiometer was positioned near the base of the wall, 24.15 cm above the canyon floor, yielding a traverse length of 72.45 cm. In the second test, the fixed radiometer was positioned 28.05 cm from

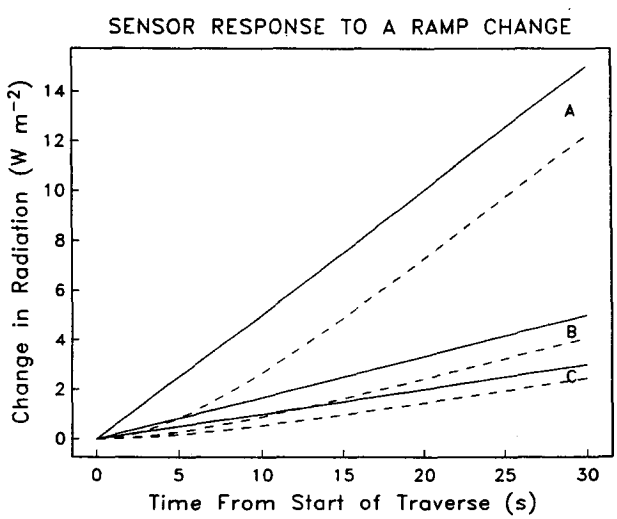

FIG. 8. Sensor response to a ramp change in L_o or L^* over a canyon wall. Total change over the wall is 30 W m^{-2}. Solid lines—actual radiation; dashed lines—measured radiation. Traverse times are: A—60 s; B—180 s; C—300 s for a 1-m canyon width.

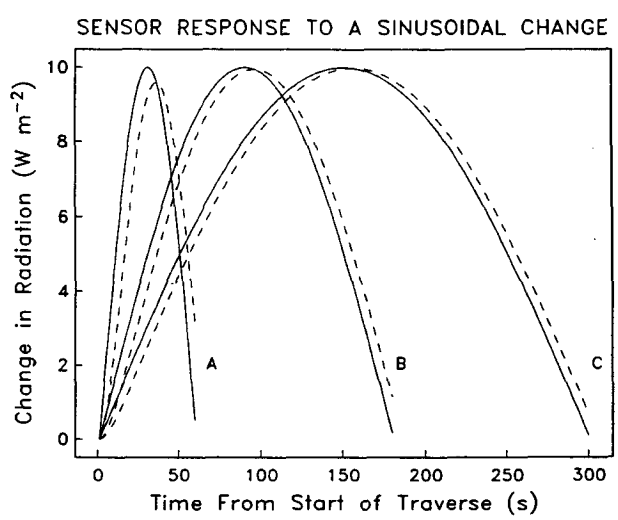

FIG. 9. Sensor response to a sinusoidal change in L_o or L^*. Solid lines—actual radiation; dashed lines—measured radiation. Traverse times are: A—60 s; B—180 s; C—300 s for a 1-m canyon width.

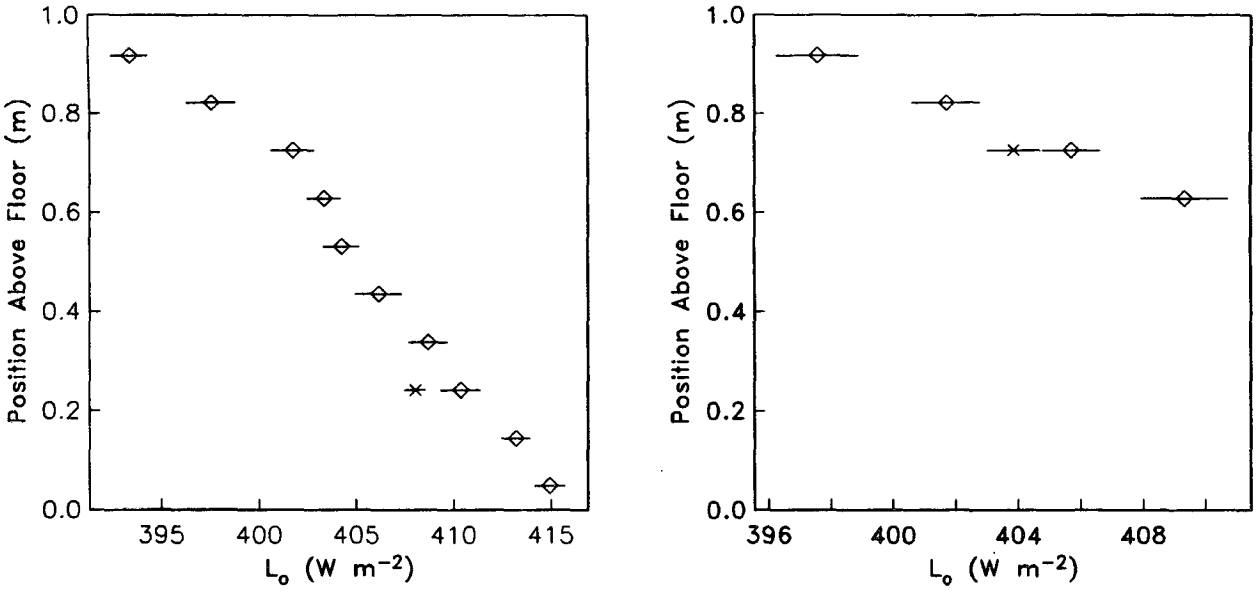

FIG. 10. Tests between a fixed (crosses) and traversed (diamonds) radiometer for L_o at (a) a position 24.15 cm from the base of the west wall and (b) 28.05 cm from the top of the wall. Error bars are standard deviations of all samples taken over each gridpoint during the traverse.

the canyon top, giving a traverse length of 24.15 cm. Traversing commenced at the top of the west wall and continued downward towards the base of the wall. The first test, which involves a greater length of traverse than that of the second, indicates an overestimate of between 2 and 3 W m^{-2}. Given the direction of traverse, and the expected distribution of radiation during this period of the evening (see Fig. 7), the tests do not produce evidence of a lag in the sensor response. A lag in response to a ramp change would produce a lower value for the traversing sensor compared to the fixed radiometer, whereas the tests indicate the opposite. It is possible with the first test that an S-shaped distribution of radiation (as illustrated in Fig. 7) could produce an overestimate of the flux density as the traversed instruments lag in their response to the decreased change in L_o. However, the chances of this occurring near the top of the wall are unlikely. It is more likely that the results are due to: (a) minor differences in the angle of the two radiometers relative to the surface they view and/or (b) the offset of the fixed radiometer from the line of traverse.

e. Specification of the instrument delay interval

The determination of sensor traversing speed based upon sensor response to the distribution of radiation across the canyon facets assumes $Q_A = Q$ at the start of a traverse across each facet. To achieve this, upon completion of a facet traverse and rotation of the sensors, the instruments must remain stationary for a period of time in order to equilibrate to the radiative environment over the new facet. The difference in radiation between two adjacent facets is equivalent to a step change. Using the time constant of the radiometers, the time needed to adjust to a given fraction of the new level of radiation may be determined from Eq. (1). Changes between facets are assumed to be greater than temporal changes occurring during the delay time.

The CTS has a built-in delay of 27 s that begins after each instrument rotation. This provides an adjustment factor of 99% based on Eq. (1). The largest changes in radiation occur during instrument rotation to and from the canyon top, with much smaller changes occurring between the walls and floor.

Confirmation of the delay interval is easily accomplished by plotting the instrument output from the radiometer after a rotation has occurred and while the CTS is in the delay phase. The step change in radiation between facets will be most clearly evident as the instrument traverse changes to and from the canyon top because of the contrast between the sky and canyon radiative temperatures. Figure 11 illustrates the adjustment that occurs over the delay period at these points. The results indicate that a 27-s delay interval is adequate for the adjustment of the sensors.

4. Conclusions

The design of a canyon traversing system that allows miniature net radiometers to be automatically moved around a model urban canyon cross section has been discussed. The speed at which the sensors move has been set according to an analysis of expected radiation distributions on canyon facets and the response of the moving sensor to them. The traverse separation dis-

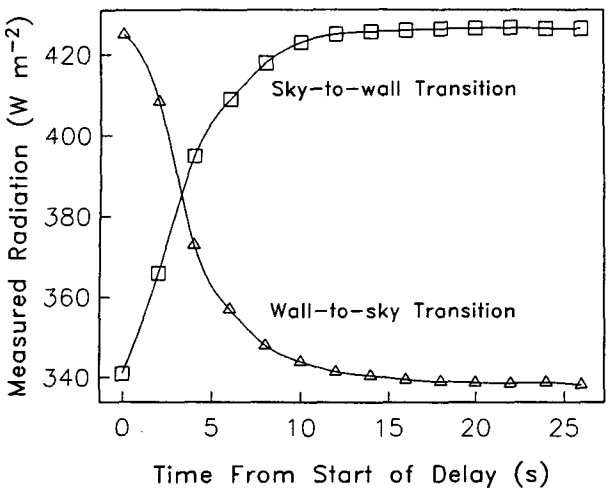

FIG. 11. Measured longwave radiation during the delay period following an instrument rotation to and from the canyon top. (L_i is measured at the canyon top, L_o from the walls.)

tance is described in relation to view-factor considerations. Tests of the traversing speed and delay length showed the design to be adequate for most conditions experienced in the model canyon.

Acknowledgments. The authors wish to thank Dr. T. R. Oke for his helpful comments. The CTS was constructed by J. Skapski and H. Kozlow of the UBC Geography Department. The field assistance of G. Frickska is acknowledged. The Department of Transport (Vancouver International Airport) made the field site available. Funding was provided by the Natural Sciences and Engineering Research Council of Canada via a scholarship to JAV and an operating grant to Dr. T. R. Oke.

REFERENCES

Aida, M., 1982: Urban albedo as a function of the urban structure—a model experiment. *Bound. Layer Meteor.*, **23**, 405–413.

Arnfield, A. J., 1976: Numerical modeling of urban surface radiative parameters. *Papers in Climatology: The Cam Allen Memorial Volume.* J. A. Davies, Ed., McMaster University, 1–28.

——, 1982: An approach to the estimation of the surface radiative properties and radiation budgets of cities. *Phys. Geogr.*, **3**, 97–122.

Fritschen, L. J., and L. W. Gay, 1979: *Environmental Instrumentation.* Springer-Verlag, 209 pp.

Idso, S. B., and K. R. Cooley, 1971: The vertical location of net radiometers. I. The effects of the underlying air layer. *J. Meteorol. Soc. Jpn.*, **49**, 343–349.

——, and ——, 1972: The vertical location of net radiometers. II. The effects of the net radiometers shadow. *J. Meteorol. Soc. Jpn.*, **50**, 49–57.

Johnson, G. T., and I. D. Watson, 1987: Modelling the radiative heating and cooling of urban canyons. *Proc. International Conf. on Modelling and Simulation.* Melbourne, Association for the Advancement of Modelling and Simulation Techniques in Enterprises, 228–234.

Monteith, J. L., 1972: *Survey of Instrumentation for Micro-Meteorology.* Blackwell, 263 pp.

Nakamura, Y., and T. R. Oke, 1988: Wind, temperature, and stability conditions in an east–west oriented urban canyon. *Atmos. Environ.* **22**, 2691–2700.

Nunez, M., and T. R. Oke, 1977: The energy balance of an urban canyon. *J. Appl. Meteor.*, **16**, 11–19.

Oke, T. R., 1981: Canyon geometry and the nocturnal urban heat island: comparison of scale model and field observations. *J. Climatol.*, **1**, 237–254.

Voogt, J. A., 1989: Validation of an Urban Canyon Radiation Model for Nocturnal Long-Wave Radiative Fluxes and the Effect of Surface Geometry on Cooling in Urban Canyons. M.S. thesis, Department of Geography, University of British Columbia, 266 pp.

——, and T. R. Oke, 1991: Validation of an urban canyon radiation model for nocturnal long-wave radiative fluxes. *Bound. Layer Meteor.*, **54**, 347–361.